CLM-P672

UKAEA

Preprint

THE BEHAVIOUR OF IMPURITIES OUT OF CORONAL EQUILIBRIUM

P. G. CAROLAN
V. A. PIOTROWICZ

CULHAM LABORATORY
Abingdon Oxfordshire
1982

CLM-P 672

THE BEHAVIOUR OF IMPURITIES OUT OF CORONAL EQUILIBRIUM

P G Carolan and V A Piotrowicz*

UKAEA, Culham Laboratory, Abingdon, Oxon., OX14 3DB, UK

(Euratom/UKAEA Fusion Association)

*Oxford Polytechnic, Headington, Oxford

ABSTRACT

The behaviour of a range of impurities, in the presence of neutral thermal hydrogen atoms, is examined analytically for non-equilibrium coronal conditions. The time, τ_{ss}, required for an impurity species to establish equilibrium is found to be sensitively dependent on the plasma electron temperature and is strongly correlated with the ionisation state distribution at equilibrium. Peak values of $n_e \tau_{ss} \simeq 2 \times 10^{18}$ m^{-3} s are found. The temporal and ensemble averaged calculations of the impurity charge states and radiation power which are presented here allow for the treatment of impurities without recourse to lengthy computation. The impurities (carbon, oxygen, iron and molybdenum) are considered in terms of the electron temperature, the fractional neutral hydrogen concentration, and the time spent by the impurities in the plasma.

(Submitted for publication in Plasma Physics)
June 1982

1 INTRODUCTION

The treatment of impurities in low density plasmas of thermonuclear interest can be exceedingly complex if account is taken of impurity transport and recycling at the walls. Since individual impurity ions, in traversing the plasma volume, may experience rapidly varying plasma conditions, there is generally insufficient time for them to reach coronal equilibrium. The time for an impurity to reach this state depends on the species considered and on the plasma electron temperature and density ($n_e \tau_{ss}$ ranges from ca. $2 \times 10^{16} - 2 \times 10^{18}$ m^{-3} s). Use of the steady-state corona model, when the impurities have spent less time than τ_{ss} in the plasma at constant temperatures, can often result in the radiated power being grossly underestimated. This happens when the impurities find themselves in lower ionisation states than those obtaining at equilibrium; the consequent increase in the ions' excitation rates usually increases the radiation power. Therefore, a determination of the impurity ionisation state distribution that considers the temporal evolution is clearly a fundamental requisite for evaluating the role played by impurities.

The problem can be tackled in several ways, most of which utilise the corona model [1] of impurities. One approach is to construct a model, that may include one or more spatial dimensions, which calculates local densities of impurity ionisation states by simulating the various transport mechanisms and atomic processes. While this method is useful, the applicability of such models is often restricted by the uncertainties which exist in some of the basic physics processes involved and by the artificiality of the boundary and initial conditions imposed, as well as the approximation of the true geometry by a simplified one. Thus the results may only apply to very specific cases.

The approach taken in this paper is to study analytically the evolution of the impurities' charge-state distributions from their moment of entry into the plasma.

Although the physical model can cope with the plasma being subjected to continually varying parameters, the results presented apply to impurities in plasmas which suffer an instantaneous electron temperature change. The value of the present treatment is that consequences of impurity contamination are immediately calculable from the results presented and a greater appreciation of the physics of the resulting plasma behaviour is therefore available.

The impurity atomic processes included in the calculations are collisional ionisation, radiative and dielectronic recombination, and the recombination by charge-exchange with neutral hydrogen atoms. The complete set of ionisation rate equations for each species (ranging from carbon to molybdenum) is solved analytically. This is preferable to a step-by-step numerical approach, with its associated stability and accuracy problems.

The evolution of the impurities is examined in terms of the ionisation state distributions and the resultant radiation power levels. By defining a quasi-steady-state that requires the mean ionic charge and the radiation power to be within 1% of their true steady-state values, we can calculate the $n_e \tau$ value required for an impurity to reach equilibrium.

We also calculate the total energy radiated at various intervals during the approach to equilibrium. Thus a temporal or ensemble averaged radiation power can be assigned to impurities whose confinement time is too short to enable them to reach coronal equilibrium.

2 THE IMPURITY IONISATION STATE DISTRIBUTION

2.1 ATOMIC PROCESSES

In the corona model, ions are excited by electron collision and then immediately decay to the ground state. As a consequence, the excitation rate coefficients are fully determined by the electron density and temperature. The radiation power is calculated from the sums of the products of the excitation rates and energies at each ionisation state which are then weighted according to the ionisation state distributions of the impurities. The essential problem in the time-dependent treatment of impurities thus consists of determining these ionisation distributions.

At plasma densities of interest (10^{18}-10^{21} m^{-3}) the dominant source of impurity ionisation is through their collision with the electrons (Lotz [2]) while the relevant recombination mechanisms are radiative (Von Goeler et al [3]), dielectronic (Burgess [4], Beigmann et al [5]), and charge-exchange with the neutral gas. Since the first three have received sufficient attention elsewhere we shall refrain from commenting further on them except to note that in this density range the rate coefficients describing them are predominantly dependent on the electron temperature. The weak density dependence of the dielectronic recombination process [6] is neglected.

At fractional neutral densities in excess of about 3×10^{-6} of the electron density, the mean ionisation state of the impurities will be so reduced, through charge-exchange recombination, that the radiation power will be noticeably enhanced (Hulse et al[7]) and so this process must also be included under such circumstances. However, a complete data set of the charge exchange cross-sections data does not

exist for a wide enough range of relative velocities (temperatures) and impurity ion states. The data that are available, however, show clear trends from which neutrals can be considered in a general fashion.

When the relative velocities between the neutrals and the impurities is low, compared with the electron orbital velocity of hydrogen in the ground state, the detailed atomic structure of the impurity must be considered in any calculation of the charge-exchange cross-section. This is especially so for light impurities (cf. Olson and Salop [8]). Furthermore, the cross-section does not have a monotonic dependence on the charge state. We have neglected such effects because of (a) the large disparity in estimates of the cross-sections at these low velocities, from the various models available and (b) the minor role played by the neutrals, as will be seen below, during the impurities' evolution to equilibrium. Their influence is most apparent in the steady-state results where, fortunately, corrections for errors in the cross-section estimates may be made.

Charge-exchange cross-sections, σ, as functions of the ionic charge, q, are illustrated in figure 1, as taken from Crandall et al [9], Hulse et al [7], Olson and Salop [8,10], and Ryufuku and Watanabe [11] for various interaction velocities, v. The disparity between the absorbing-sphere-model of Olson and Salop (OSAS) [10] and the universal-unitarised-distorted-wave-approximation (UUDWA) of Ryufuku and Watanabe [11], especially at low q, is largely due to two effects: (a) the OSAS curves represent maxima in cross-section at each q value for a range of atomic numbers considered, and (b) the UUDWA is an averaged curve computed from many UDWA profiles covering a wide range of elements (cf. figure 2). In addition, the OSAS model generally gives larger cross-section values, especially for lighter elements, than do other models (e.g. Salop and Olson's 6-molecular state model [12] and the Vaben and Briggs 11-molecular state model [13] which gives the closest agreement with experimental values of $C^{6+} + H \rightarrow C^{5+} + H^{+}$ of Crandall et al [14]). However, recent experimental results of Crandall et al [9] (cf. experimental points in figure 1) show

that the OSAS model overestimates σ by, at most, a factor of 2 at q = 3 and $v = 4\times10^5 ms^{-1}$ but typically overestimates by < 30% for higher q values. This discrepancy hardly affects the results because of the much higher ionisation and dielectronic recombination rates compared with the charge-exchange recombination rates of low ionic charge states.

In the results presented below we have used the scaling appropriate to the OSAS model at $v_1 = 2\times10^5 ms^{-1}$ which gives a $q^{\frac{3}{4}}$ dependence (cf. figure 1). In general, of course, the true $\langle\sigma v\rangle$ cross-sections will differ from those used in the computations. However, this can be rectified by applying a correction factor, $\varepsilon = \langle\sigma v\rangle/\sigma_1 v_1$, to the fractional neutral abundance. We may then write for the charge-exchange recombination rate coefficient

$$\alpha_{cx} = \varepsilon \frac{n_o}{n_e} \sigma_1 v_1 \qquad (1)$$

where $\sigma_1 v_1 = 5.5\times10^{14} q^{\frac{3}{4}} m^3 s^{-1}$, n_o is the neutral hydrogen density, and n_e is the electron density.

2.2 THE IONISATION RATE EQUATIONS

The ionisation rate equations describe the net effect of the ionisation and recombination processes, and of transport. Neglecting the latter, they are written as

$$\frac{dy_1}{dt} = n_e (-y_1 S_1 + y_2 \alpha_2)$$

$$\frac{dy_k}{dt} = n_e (y_{k-1} S_{k-1} - y_k (S_k + \alpha_k) + y_{k+1} \alpha_{k+1}) \qquad (2)$$

$$\frac{dy_{z+1}}{dt} = n_e (y_z S_z - y_{z+1} \alpha_{z+1})$$

where y_k = the fractional abundance of the k'th ionisation state = $n_{I,k}/n_I$

n_I = the impurity density

$n_{I,k}$ = the impurity density at the k'th ionisation state

S_k = the ionisation rate coefficient from state k to k+1

α_k = the recombination rate coefficient from state k to k-1

Z = the atomic number

It is computationally convenient to symmetrise the rate matrix by replacing the fractional abundances, y_k, with new variables, v_k, according to the transformation

$$v_k = T_k\, y_k \qquad T_k = \begin{cases} 1 & k = 1 \\ \left(\dfrac{\alpha_2\alpha_3 \cdots \alpha_k}{S_1 S_2 \cdots S_{k-1}}\right)^{\frac{1}{2}} & k > 1 \end{cases} \tag{3}$$

We then have

$$\frac{dv_1}{dt} = n_e\,(-v_1 S_1 + v_2\sqrt{S_1\alpha_2})$$

$$\frac{dv_k}{dt} = n_e\left(v_{k-1}\sqrt{S_{k-1}\alpha_k} - v_k(S_k + \alpha_k) + v_{k+1}\sqrt{S_k\alpha_{k+1}}\right) \tag{4}$$

$$\frac{dv_{k+1}}{dt} = n_e\,(v_z\sqrt{S_z\alpha_{z+1}} - v_{z+1}\,\alpha_{z+1})$$

which can be written in matrix notation as

$$\frac{d\underline{v}}{dt} = n_e\,\underline{\underline{A}}\,\underline{v} \tag{5}$$

where $\underline{\underline{A}}$ is the tridiagonal symmetric matrix given by

$$\underline{\underline{A}} = \begin{pmatrix} -S_1 & \sqrt{S_1\,\alpha_2} & 0 & \cdot\cdot \\ \sqrt{S_1\,\alpha_2} & -(S_2+\alpha_2) & \sqrt{S_2\,\alpha_3} & \cdot\cdot \\ 0 & \sqrt{S_2\,\alpha_3} & \cdot\cdot\cdot & \\ \cdot & \cdot & & \\ \cdot & \cdot & & \end{pmatrix} \qquad (6)$$

It is then assumed that the solution vector $\underline{v}$ is of the form

$$\underline{v} = \sum_i a_i\,\underline{x}_i \exp\,(n_e\,\lambda_i\,t) \qquad (7)$$

which on substitution into equation (5) gives

$$\sum_i a_i\,n_e\,\lambda_i\,\underline{x}_i \exp\,(n_e\,\lambda_i\,t) = \sum_i a_i\,n_e\,\underline{\underline{A}}\,\underline{x}_i \exp\,(n_e\,\lambda_i\,t) \qquad (8)$$

The non-trivial solution to equation (8) requires that

$$(\underline{\underline{A}} - \lambda_i\,\underline{\underline{I}})\;\underline{x}_i = 0 \qquad (9)$$

and thus equation (7) is the solution of equation (4) if λ_i are the eigenvalues and $\underline{x}_i$ are the eigenvectors of the matrix $\underline{\underline{A}}$. In order to calculate the constants a_i it is necessary to consider the solution at t = 0 i.e.

$$\underline{v}_o = \sum_i a_i\,\underline{x}_i \qquad (10)$$

The vector $\underline{v}_o$ depends on the values assigned to the impurity initial fractional abundances (e.g. $v_1 = 1$, $v_k = 0$ for $k > 1$ in the case of neutrals). Recalling that the matrix $\underline{\underline{A}}$ is symmetric and, therefore, that its eigenvectors are identical to those of its transpose, pre-multiplying equation (10) by $\underline{x}'_r$, the transpose of $\underline{x}_r$, and invoking the orthogonality relationship which exists between the eigenvectors of a matrix and those of its transpose gives

$$\underline{x}'_r\;\underline{v}_o = a_r\,\underline{x}'_r\,\underline{x}_r = a_r \qquad (11)$$

It is interesting to consider one of the consequences of this solution. As the system of equations (2) is conservative the matrix $\underline{\underline{A}}$ is singular and one of its eigenvalues is, therefore, zero. The other eigenvalues are all negative, so the eigensolution corresponding to this zero eigenvalue becomes dominant as $t \to \infty$. This is none other than the steady-state solution corresponding to the temperature at which the elements of the matrix $\underline{\underline{A}}$ are evaluated, i.e.

$$\frac{y_{k+1}}{y_k} = \frac{S_k}{\alpha_{k+1}} \tag{12}$$

3 THE RADIATED POWER AND MEAN CHARGE OF IMPURITIES

Impurities in plasmas give rise to line and recombination radiation in addition to enhancing the bremsstrahlung. The power, P, radiated by a particular impurity species may be written as

$$P = \sum_k P_{k\ell} + P_{kr} + P_{kd} + P_{kc} + P_{kBr} \tag{13}$$

where $P_{k\ell}$ is the line radiation from impurities in the k'th state

P_{kr} is the radiative recombination radiation

P_{kd} is the dielectronic recombination radiation

P_{kc} is the charge-exchange recombination radiation

P_{kBr} is the bremsstrahlung due to the impurities

We will now deal with these separately.

(a) Line Radiation

In the corona model excited ions are assumed to undergo instantaneous radiative decay. Thus the line radiation is given by the product of the ion abundances, the excitation rates, and the transition energies. We have

$$P_{k\ell} = n_e n_I y_k \sum_{n=1}^{n} Q_{kn} \Delta E_{kn} \qquad (14)$$

where N is the the number of transitions included (typically 1-10)

Q_{kn} is the the excitation rate coefficient of the n'th transition

ΔE_{kn} is the the excitation energy of the n'th transition

(b) Radiative Recombination Radiation

In this process a free electron is captured by an ion; the kinetic energy of the electron and the potential energy of the recombined ion is radiated, to give, on average

$$P_{kr} = n_e n_I y_k \alpha_{rr_k} (\chi_{k-1} + \langle E_e \rangle) \qquad (15)$$

where χ_{k-1} is the ionisation potential of the recombined ion

$\langle E_e \rangle$ is the average kinetic energy of the recombining electrons

(c) Dielectronic Recombination Radiation

When the energy of an electron is below the excitation threshold energy it can excite an ion and subsequently find itself with insufficient energy to escape from the ion's Coulomb field. If the excited electron decays radiatively (the stabilising transition) then the colliding electron is captured. The radiation which results is

$$P_{kd} = n_e n_I y_k \alpha_{dr_k} (\chi_{k-1} + E_k) \qquad (16)$$

where E_k is the excitation energy of the resonant transition.

The atomic data used for the above processes are as used in the MAKOKOT code (Equipe TFR [15]) except for the lower ionisation stages of iron (Fe I to Fe VII) where the values are taken from Uchikawa et al [16] and molybdenum (Mo I to Mo XXIII) where the relevant data are calculated using the Average Ion Model of Post [17].

(d) Charge-exchange Recombination Radiation

The charge-exchange electron will be in an excited state immediately following the collision. However, there will be a range of principal quantum states available with associated differential cross-sections (cf Ryufuku and Watanabe [11]). This makes the radiation calculations exceedingly difficult, especially as most of the data available at present are for fully ionised impurities. Nevertheless, when we assume, in the manner of Hulse et al [7], that on collision the full ionisation potential of the recombined ion is radiated, we find that this loss is less than the additional power radiated as a result of the altered charge-state distribution. Thus we have

$$P_{kc} = n_e n_I y_k \alpha_{cx_k} \chi_{k-1} \qquad (17)$$

(e) Bremsstrahlung

The additional bremsstrahlung power due to the presence of a particular impurity charge-state is

$$P_{k_{Br}} = 1.53 \times 10^{-38} n_e n_I y_k T_e^{\frac{1}{2}} (k - 1)^2 \ Wm^{-3} \qquad (18)$$

(f) The Mean and Mean Square Charge

The quantities $\langle Z \rangle$ and $\langle Z^2 \rangle$ are used to calculate the number of additional free electrons produced when impurities are ionised, and the enhancement of the plasma resistivity and bremsstrahlung; we have, by definition,

$$\langle Z \rangle = \sum_k y_k (k - 1) \qquad (19)$$

$$\langle Z^2 \rangle = \sum_k y_k (k-1)^2 \qquad (20)$$

The increase in the electron density, Δn_e, is simply

$$\Delta n_e = \sum_I n_I \langle Z \rangle_I \qquad (21)$$

In addition, the plasma can be considered to be composed of ions of an effective ionic charge, Z_{eff}, when calculating the resistivity and the total bremsstrahlung. This is defined as

$$Z_{eff} = \frac{n_i + \sum_I n_I \langle Z^2 \rangle_I}{n_e} \qquad (22)$$

where n_i is the proton density.

(In practice $\langle Z^2 \rangle$ need not be calculated independently since, with good accuracy, we may write $\langle Z^2 \rangle = \langle Z \rangle^2$, for $\langle Z \rangle > 1$, and $\langle Z^2 \rangle = \langle Z \rangle$, otherwise.)

4 RESULTS

We have considered a range of impurities from low Z (carbon) to high Z (molybdenum), and examined their behaviour for a range of neutral densities under the headings steady-state time, average charge, and radiation. The sequence of events followed in our calculations is one in which the impurities are introduced as neutrals to a region of steady electron temperature or, equivalently, where starting with a cold plasma, a constant temperature is reached in a time much shorter than that required for the impurities to reach steady-state. Since the first few electrons are shed rapidly from the impurities, (typically in a few μs at $n_e \simeq 10^{19}$ m^{-3}) it makes little difference to the results presented below if, alternatively, they are initially partially ionised. The only proviso is that the

initial ionisation state distribution is similar to those found at temperatures somewhat less than that at which the first radiation peak occurs. (When impurities are introduced with a coronal equilibrium distribution characteristic of some arbitrary temperature, we find that the results are accurate only for temperatures beyond that at which the next radiation peak occurs.)

This approach is of particular relevance to the start up phase and, also, to the edge regions of plasmas (cf McCracken and Stott [18]) where there may be rapid recycling of impurities. These emerge from the wall (predominantly as neutrals) radiate as they are ionised, and finally return to the wall where they are neutralised.

(a) Steady-state Time

Clearly, the treatment of impurities is greatly simplified when they can be considered to be in coronal equilibrium. Data are available from many authors (e.g.Post [17]) which describe, for such impurities, the average ion state and power radiated, over a wide range of electron temperature, for many elements. It is therefore of some interest to calculate the time required for impurities to reach such a steady-state.

Steady-state conditions rarely exactly obtain but, for most practical purposes, we may define such a state to exist when P and $\langle Z \rangle$ of the impurity in question are each within 1% of their true coronal equilibrium values. It is apparent from the ionisation rate equations that the factors which determine the evolution of the impurities are the initial ionisation state distribution, the neutral hydrogen density, the electron temperature, T_e, and the time integral of the electon density. We usually represent the latter by the quantity $n_e\tau$, which is convenient since the quality of plasma confinement is often judged in terms of $n_e\tau_E$ and $n_e\tau_p$ where τ_E and τ_p are the energy and particle confinement times respectively, of the electrons and

ions. (Of course, the appropriate independent variable is $n_e t$ and, in fact, $(n_e \tau)_{ss}$ is calculated.)

The $n_e \tau$ values required for initially neutral impurities to reach steady-state, as defined above, are shown in figures 3(a) to 6(a). It can be seen that the $n_e \tau_{ss}(T_e)$ functions of the various impurity elements are markedly different both in terms of the temperatures at which the peaks and troughs occur, and in the amplitude of variation. The height of the peaks of the light impurities are all of similar magnitude ($\sim 2 \times 10^{18}$ m^{-3} s) in contrast to those of the heavy impurities where the peaks at low temperatures are substantially less than the high temperature peak. Although the maximum $n_e \tau_{ss}$ peak of molybdenum, for example, is comparable in magnitude to the carbon or oxygen peaks, the low temperature (110 eV) peak is an order of magnitude lower.

When an envelope is taken of the ionisation distributions shown in figures 3(b) to 6(b) a strong correlation is seen between these and the $n_e \tau_{ss}$ functions. The relatively small values of $n_e \tau$ required to reach steady-state for the He-like, Ne-like, and Ni-like ions is a result of the large difference in ionisation potential between that of a single electron shell state and a closed shell state. The reduced ionisation rate prevents the next state (i.e. closed shell minus one electron) from being heavily populated and the dielectrionic recombination rate, which exceeds the radiative recombination rate, is also severely reduced. Both of these factors ensure the rapid population of the closed shell configurations. Thus a minimum in $n_e \tau_{ss}$ will be found at those temperatures where closed shell configurations predominate, i.e. where the envelope of the ionisation distribution has maxima.

The presence of hydrogen neutrals, even in small quantities, can reduce the $n_e \tau_{ss}$ values, as seen in figures 3(a) to 6(a). A general shift of peaks and troughs to higher temperatures is also observed. This is a result of the increased recombination rate necessitating an enhanced ionisation rate, and hence higher

temperatures, to establish similar ionisation state distributions. The overall reduction in $n_e\tau_{ss}$ is principally due to the general lowering of the average equilibrium ionisation state, i.e. a neutral impurity does not have so far to go, in terms of ionisation state.

(b) Impurity Temporal Behaviour

(i) Average Charge

The evolution of the mean charge-state <Z> of the various impurities is shown in figures 3(c) to 6(c). When neutral hydrogen is included only the equilibrium values of <Z> are calculated, since then the evolutionary behaviour preceeding equilibrium is so similar to that in the absence of neutrals.

It can be seen that as $n_e\tau$ is increased the ionisation states which are first to reach their steady-state are those whose ionisation distribution curves are broadly peaked at steady-state. As a result of the increased recombination rate, a general shift of ionisation state to higher temperatures is seen as the fractional neutral density is increased. It is of interest to note that at very small $n_e\tau$ values the slope of the <Z> function is negative at high temperatures; this is a reflection of the similar behaviour in the ionisation rates of the lower charge states.

(ii) Radiation Power Function

The power that the impurities radiate, as a function of $n_e\tau$, is shown in figures 3(d) to 6(d). Only in the lower Z impurity cases is there a strong correlation between minima in radiation power and closed shell configurations (cf <Z> curves). The reasons for this are as follows. An examination of figures 3(b) to 6(b) shows that as the impurity atomic number, Z, is increased a merging of ionisation state distributions occurs in the vicinity of closed shells. This merging

of states is due to the fall-off in the fractional separation of ionisation potentials of the neighbouring ion states as Z is increased. Since closed shell configurations radiate least, due to their relatively high excitation energies, the minima in radiation from high Z impurities are less pronounced and more displaced with respect to the closed shell. It is quite evident from the figures that the farther the impurities are from coronal equilibrium (i.e. small $n_e\tau$ values) the flatter the radiation curves are. I.e., the closely packed ionisation states, which are the strongest radiators, must be 'burnt-through' to reach the closed shell configurations. It follows that considerable enhancement of radiation, over that of steady-state, will usually occur only at temperatures in excess of that of the first radiation peak.

The plasma electron temperature at which a time-dependent treatment of the impurities becomes necessary in order to accurately determine the radiation power can be found on examination of figures 3(d) to 6(d). Clearly for low-Z elements this temperature is simply that of the first radiation peak; if temperatures above this are of interest then the coronal equilibrium model is of only limited use. For high-Z elements no such clear-cut temperature exists, though there are obviously regions where the equilibrium model would probably be sufficiently accurate.

The presence of neutrals has little effect on power functions at low T_e or low $n_e\tau$ values. This is primarily because the charge-states under such conditions are low. Thus (a) the charge-exchange cross-section reaction rates, which go as $q^{\frac{3}{4}}$, are low, and (b) the increasingly large effect on a given charge-state due to the cumulative effects of charge-exchange on the lower states is still small. However where both T_e and $n_e\tau$ are large there is an increase in the radiation level for even small fractions of neutrals (strictly speaking small $\varepsilon n_o/n_e$ values). This is because the increased recombination rates make the ionisation distributions (figures 3(b) to 6(b)) less irregularly dependent on the temperature. The relatively large

temperature range occupied by the closed shell states is encroached upon by adjacent ion states. Since these states can radiate orders of magnitude more power than closed shell states, a small increase in their population, through charge-exchange, can considerably increase the radiated power.

(c) Temporal and Ensemble Averaging of <Z> and Radiated Power

The above results are most relevant to the case where a study is required of the temporal behaviour of a particular batch of impurities which enters the plasma at a specific time. It may be important, for instance, to determine the period an impurity must spend in a plasma, to reach a particular ionisation state, in order to account for the experimentally observed history of lines. The simplest case to treat would be that where impurities are present ab initio with no further influx throughout the period of interest.

To calculate the total energy radiated at specific temperatures we perform a temporal integral of the radiation power function. The average radiated power is obtained on dividing this by the integration period. In plasma devices where the impurity content is largely determined by the starting conditions (e.g. base pressure or inital wall content) economies in the plasma losses may be made through suitable temperature programming which takes such averaged data into account.

However, the temporal averaging of the data can be viewed usefully in a much broader context. In most plasmas there will be an ensemble of impurities which have entered the plasma at different times. We assume a simple particle confinement model where individual impurities spend identical periods of time in the plasma. A temporal averaging is therefore exactly equivalent to an ensemble averaging, provided that the particle densities remains constant throughout the integration period. In such cases the integration period is to be interpreted as the impurity particle confinement time.

(i) Average Charge

The time-averaged charge of a batch of impurities in a plasma is

$$\langle \bar{z} \rangle = \frac{1}{n_e \tau} \int_0^{n_e \tau} \langle z \rangle \, (n_e t) \quad d(n_e t) \tag{23}$$

and substituting equations 19, 3 and 7, and integrating, this becomes

$$\langle \bar{z} \rangle = \frac{1}{n_e \tau} \sum (k - 1) \, T_k^{-1} \left\{ a_N x_N^{\,k} n_e \tau + \sum_{i \neq N} \frac{a_i}{\lambda_i} \, x_i^{\,k} \quad \left[\exp \, (n_e \lambda_i \tau) - 1 \right] \right\} \tag{24}$$

where the subscript N denotes the steady-state component. This quantity is plotted in figures 3(e) to 6(e) for the various impurities.

(ii) Average Radiation Power

The total energy, E_I, that a single impurity will radiate in time τ is

$$E_I = \int_0^{n_e \tau} \frac{P_I}{n_e n_I} \quad d(n_e t) \tag{25}$$

Writing

$$\frac{P_I}{n_e n_I} = \sum_k y_{k,I} \, R_{k,I} \tag{26}$$

where R_k are the total radiation coefficients. Equation 25 becomes

$$E_I = \int_0^{n_e \tau} \sum_k y_k \quad R_k \quad d(n_e t)$$

$$= \sum_k T_k^{-1} \, R_k \left\{ a_N \, x_N^{\,k} \, n_e \tau + \sum_{i \neq N} \frac{a_i}{\lambda_i} \, x_i^{\,k} \, \left[\exp \, (n_e \lambda_i t) - 1 \right] \right\} \tag{27}$$

The average power radiated, $\bar{P}_I$, per unit volume is then given by

$$\bar{P}_I = \frac{n_I E_I}{\tau} \qquad (28)$$

The results of the calculations are shown in figures 3(f) to 6(f) where the normalised radiation power, $\bar{P}_I/(n_e n_I) = E_I/(n_e \tau)$ is plotted against T_e in the usual way.

5 CONCLUSIONS

The time, τ_{ss}, that impurities must spend in a plasma before reaching coronal equilibrium has been computed for a wide range of electron temperatures and impurity elements. The evolution of the impurities during the non-equilibrium phase has been examined and the radiated power and average ion state have been calculated as functions of T_e, $\int_0^\tau n_e(t)dt$, and n_o. (τ is the period spent by the impurity in the plasma; n_o is the neutral hydrogen density.) It is shown that when impurities are introduced into plasmas whose temperatures give closed shell ionic configurations at equilibrium, the time τ_{ss} is minimised. However, since such configurations radiate least, the initial radiation power can greatly exceed the final value.

The power radiated from an ensemble of impurities, which have entered the plasma at different times, but which have identical confinement periods, is calculated from a simple temporal averaging of the radiation power functions. When $\tau \ll \tau_{ss}$ there is little fall-off in the radiated power at temperatures exceeding that at which maximum radiation is observed at equilibrium (e.g. T_e = 20 eV for oxygen). This is in contrast to the equilibrium situation where there are generally orders of magnitude difference between maximum and minimum radiation power levels. Thus local or transient radiation losses in plasmas can greatly exceed those at coronal equilibrium. This is of particular significance in the case of iron where, even at

low temperatures (several eV), the power radiated was found to exceed that of oxygen by a factor of over 20 at $n_e \tau \lesssim 10^{18}$ m^{-3} s.

REFERENCES

[1] McWHIRTER R W P: Plasma Diagnostic Techniques, ed R H Huddlestone and S L Leonard, Academic Press, New York (1965)

[2] LOTZ W: Internal Reports, Max-Planck-Institut, Garching, IPP 1/62 (1967) and IPP 1/76 (1968)

[3] VAN GOELER S, STODIEK W, EUBANK H, FISHMAN H, GREBENSHCHIKOV S and HINNOV E: Nuclear Fusion 15 (1975) 301

[4] BURGESS A: Astrophysics J 141 (1965) 1588

[5] BEIGMANN I L, VAINSHTEIN L A and SYUNYAEV R A: Soviet Physics Usp 11 (1968) 411

[6] ZHDANOV V A: Sov. J Plasma Physics 5 (1979) 320

[7] HULSE R A, POST D E, MIKKELSON D R: Princeton Plasma Physics Laboratory Report (1980) PPPL 1633

[8] OLSON R E and SALOP A: Phys Review A14 (1976) 579

[9] CRANDALL D H, PHANEUF R A and MEYER F W: Phys Rev A22 (1980) 379

[10] OLSON R E and SALOP A: Phys Rev A16 (1977) 531

[11] RYFUKU H and WATANABE T: Phys Rev A20 (1979) 1828

[12] SALOP A and OLSON R E: Phys Rev A16 (1977) 1811

[13] VAABEN J and BRIGGS J S: J Phys B10 (1977) L521

[14] CRANDALL D H, PHANEUF R A and MEYER F W: Phys Rev A19 (1979) 504

[15] Equipe TFR: "MAKOKOT". MERCIER et al (1977)

[16] UCHIKAWA S, GRIEM H R and DÜCHS D: IPP 6/199 (1980)

[17] POST D E, JENSEN R V, TARTER C B, GRASBERGER W H and LOKKE W A: At. Data and Nuc Data Tables 20 (1977) 397

[18] McCRACKEN G M and STOTT P E: Nuclear Fusion 19 (1979) 889

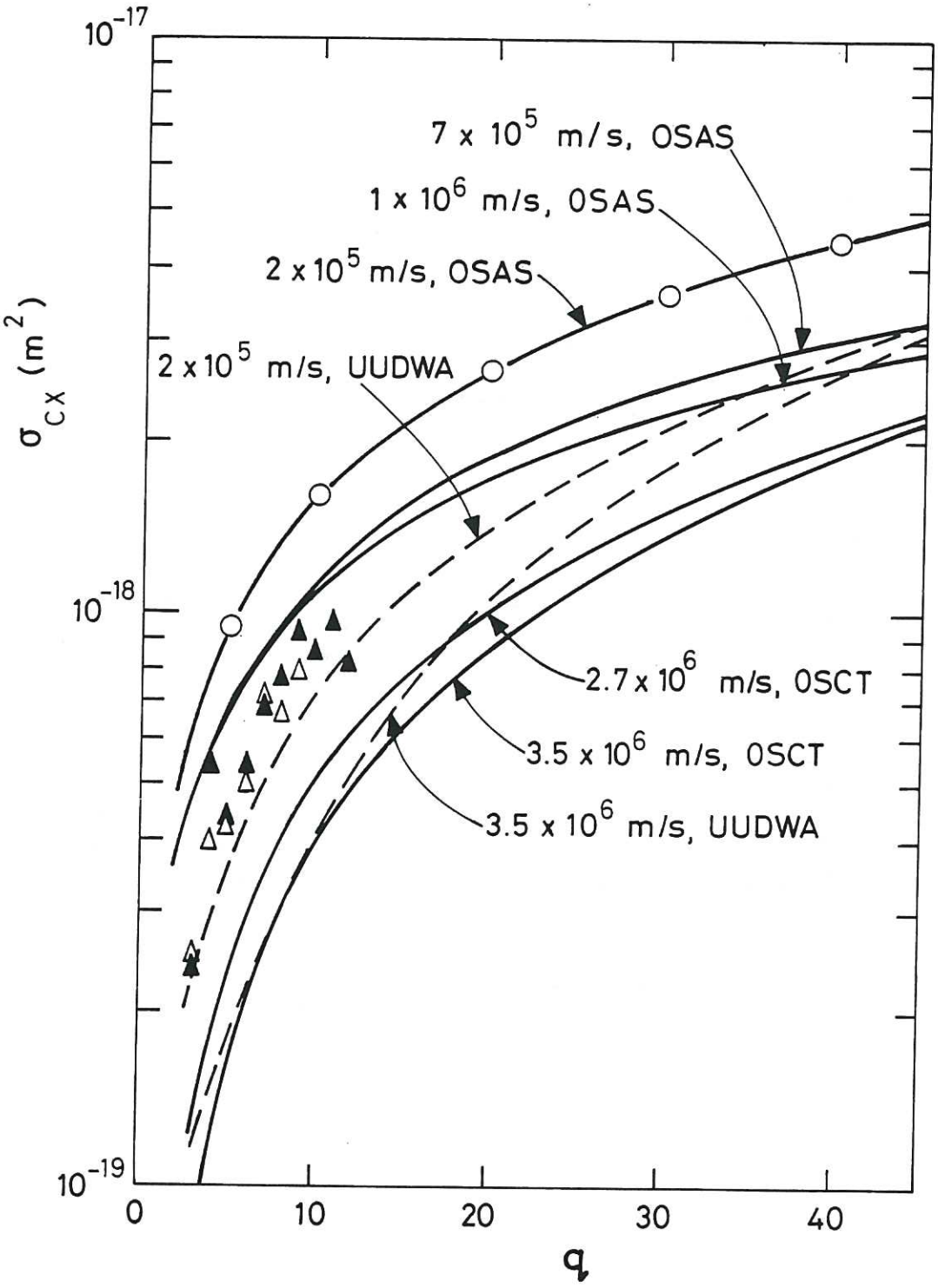

Fig.1 Charge-exchange cross-sections, σ_{cx}, as functions of the ionic charge q, for a range of relative velocities. The models used are (i) the absorbing-sphere model of Olson and Salop (OSASO) [10] (ii) the classical trajectory model of Olson and Salop (OSCT) [8] (iii) the universal-unitarised-distorted-wave-approximation (UUDWA) of Ryufuku and Watanabe [11].
Recent experimental points from Crandall et al [14] are also shown for Xenon (△) and Argon (△) where the relative velocity of the ions and the neutrals was 4×10^5 ms^{-1}. The open circles correspond to a $q^{3/4}$ best fit.

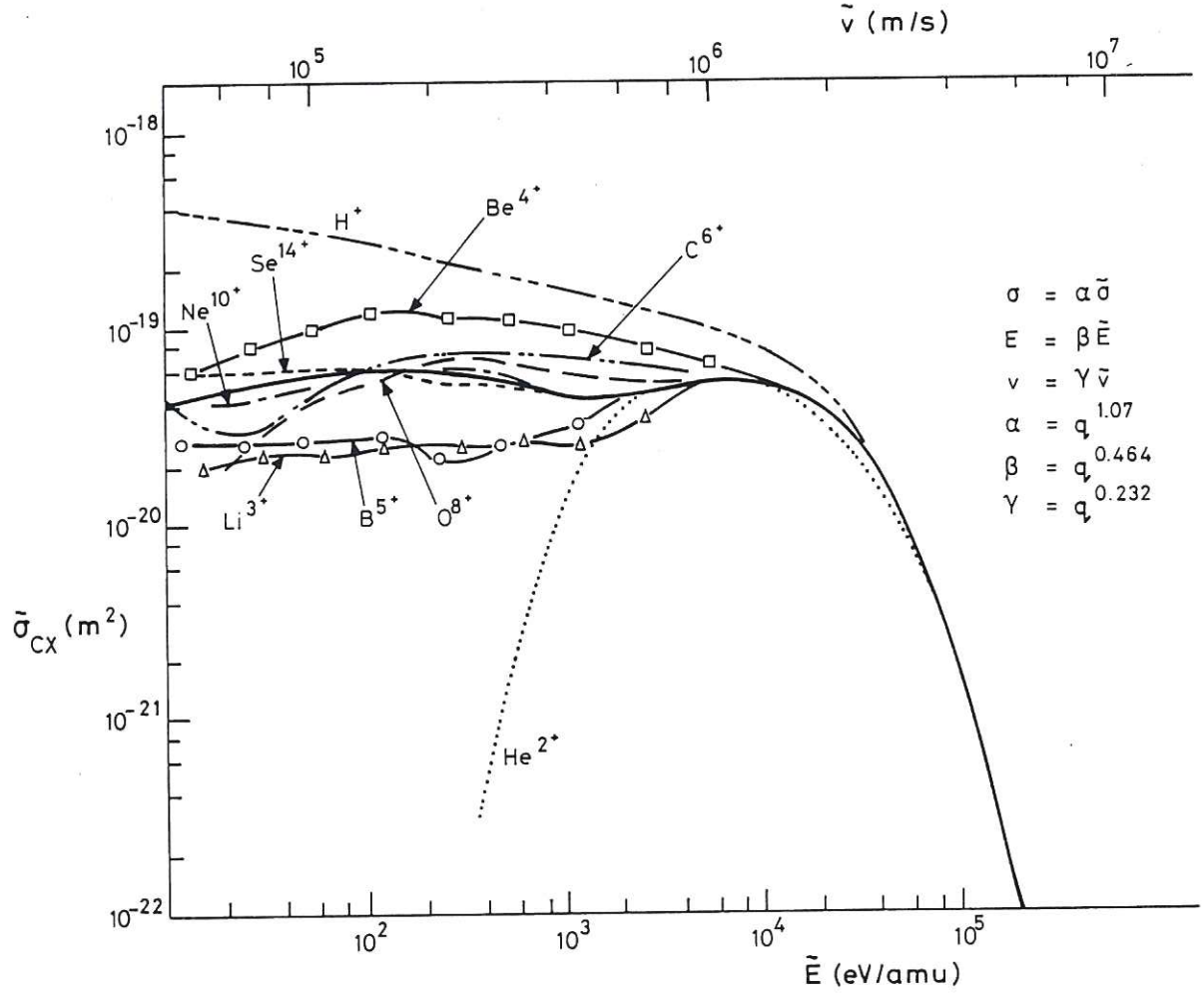

Fig.2 Charge-exchange cross-section, σ_{cx}, as a function of the relative velocity or energy for fully ionised ions up to Si^{14+}.

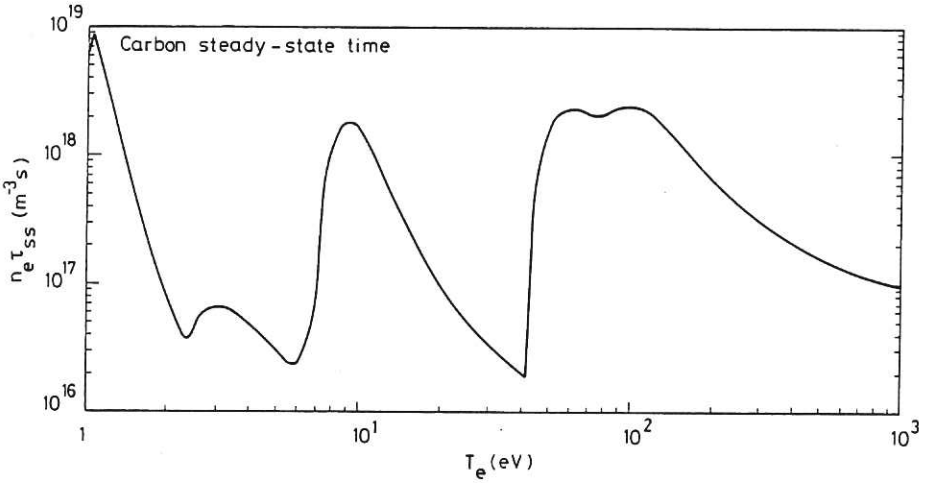

Fig.3(a) The $n_e\tau$ values for carbon to reach a steady-state.

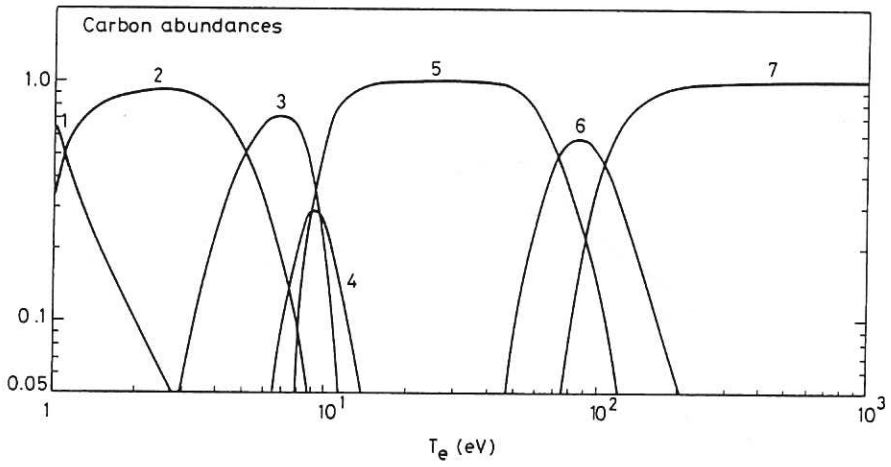

Fig.3(b) The carbon equilibrium ionisation state distribution.

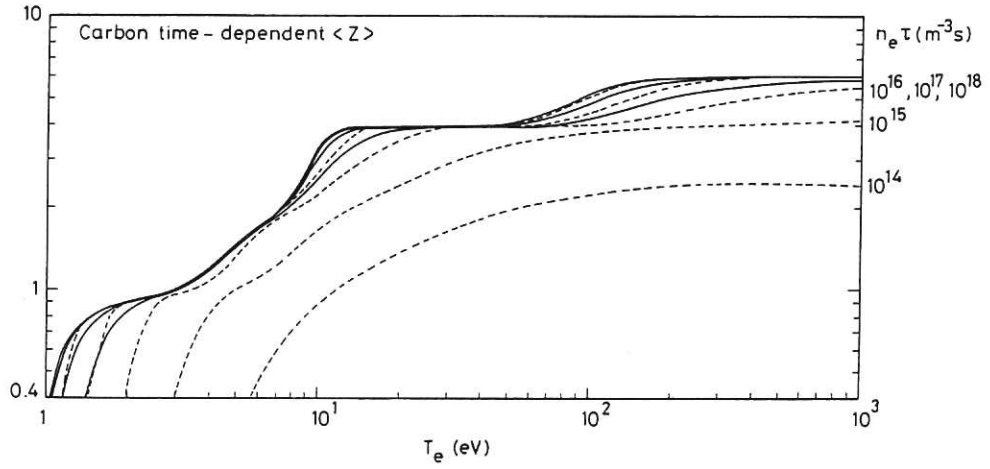

Figure 3(c).

Fig.3(c) The carbon mean ionic charge, <Z>, at various values of $n_e\tau$(----) and the equilibrium values with neutral hydrogen present (——).

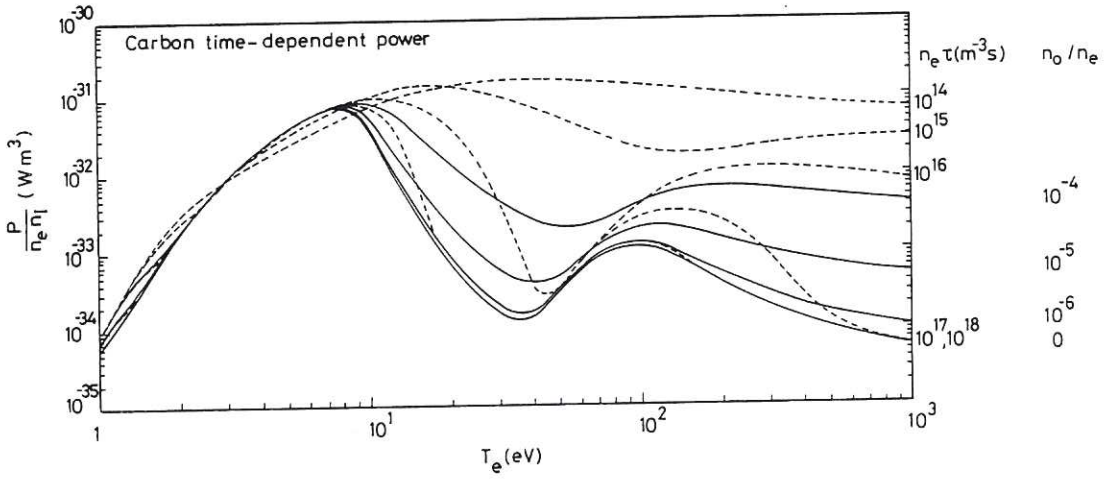

Fig.3(d) The carbon radiation power functions, $P/(n_e n_I)$, at various values of $n_e\tau$ (----) and the equilibrium functions with neutral hydrogen present (——).

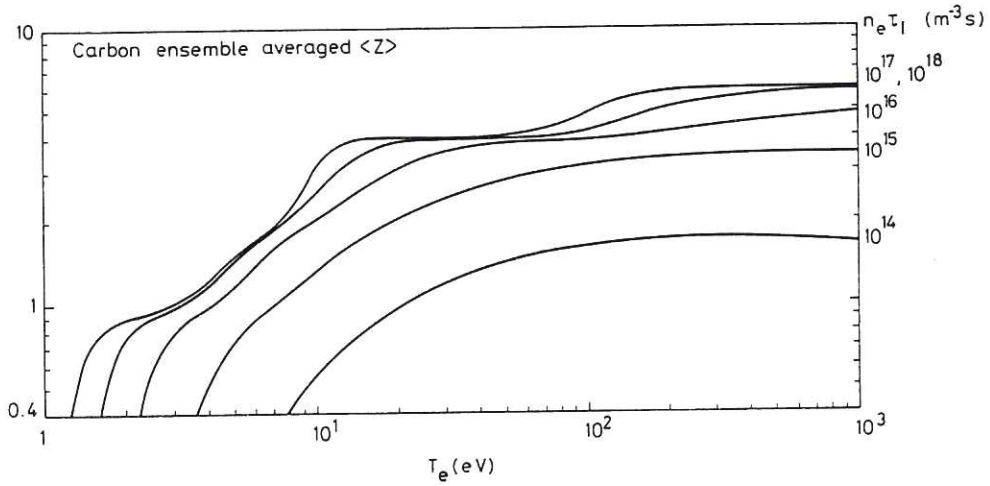

Fig.3(e) The carbon time or ensemble averaged ionic charge, $<Z>$, for various values of τ_I (the impurity ion confinement time, or time in plasma).

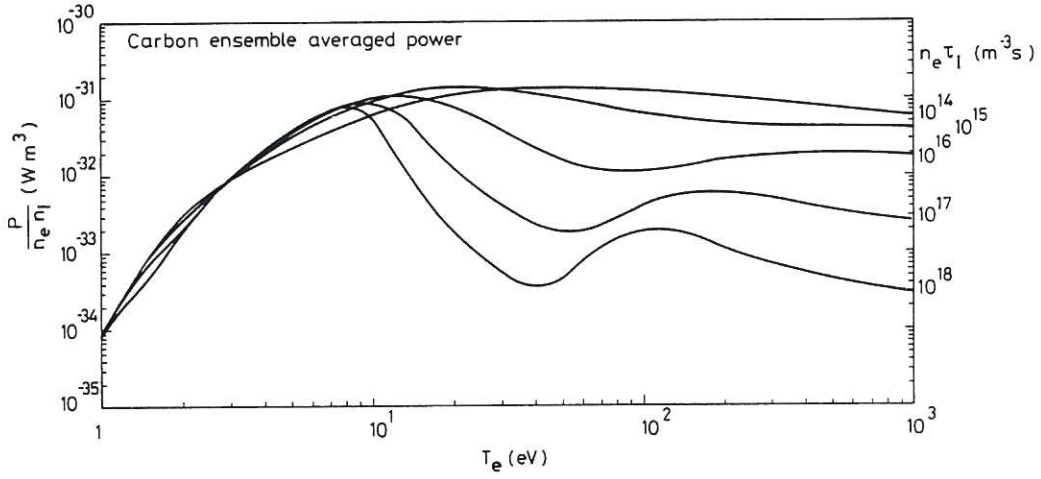

Fig.3(f) The carbon time or ensemble averaged radiation power functions, $P/(n_e n_I)$, for various values of τ_I (the impurity ion confinement time, or time in plasma).

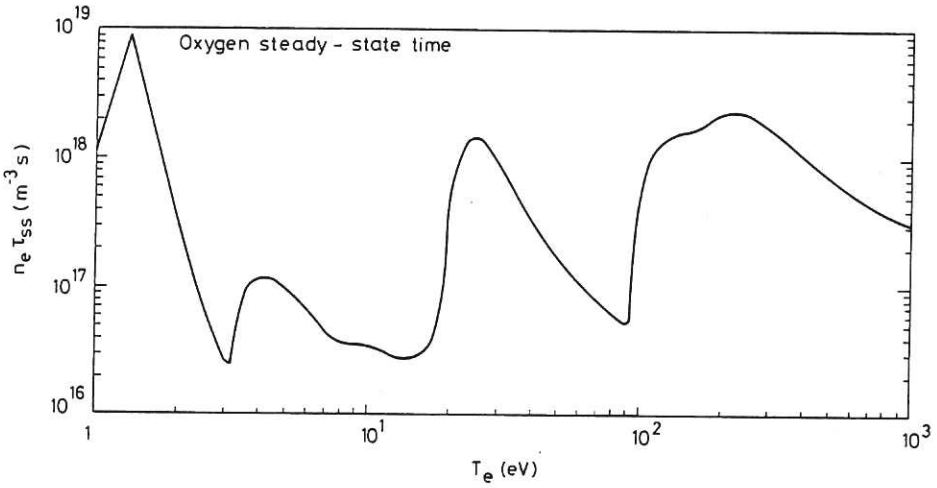

Fig.4(a) The $n_e\tau$ values for oxygen to reach a steady-state.

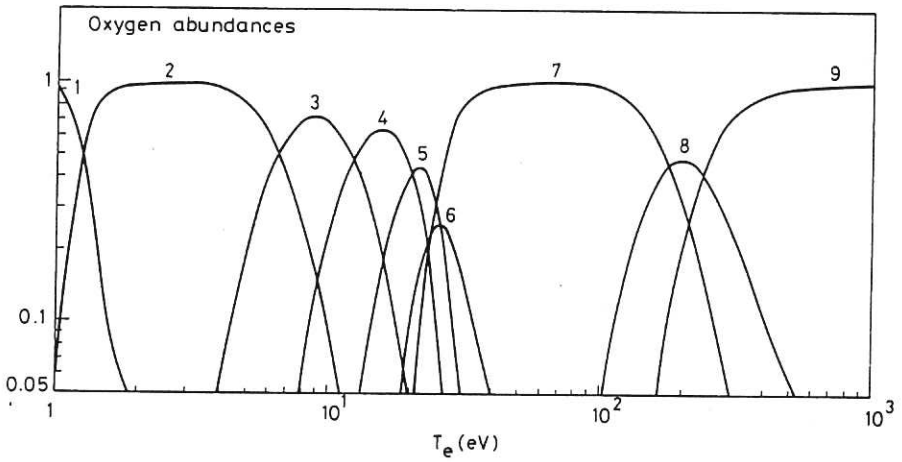

Fig.4(b) The oxygen equilibrium ionisation state distribution.

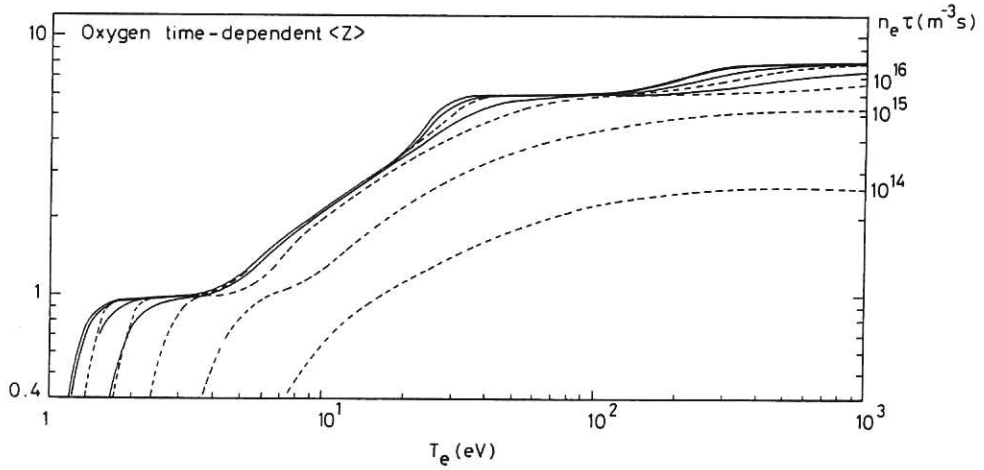

Fig.4(c) The oxygen mean ionic charge, <Z>, at various values of $n_e\tau$(----) and the equilibrium values with neutral hydrogen present (——).

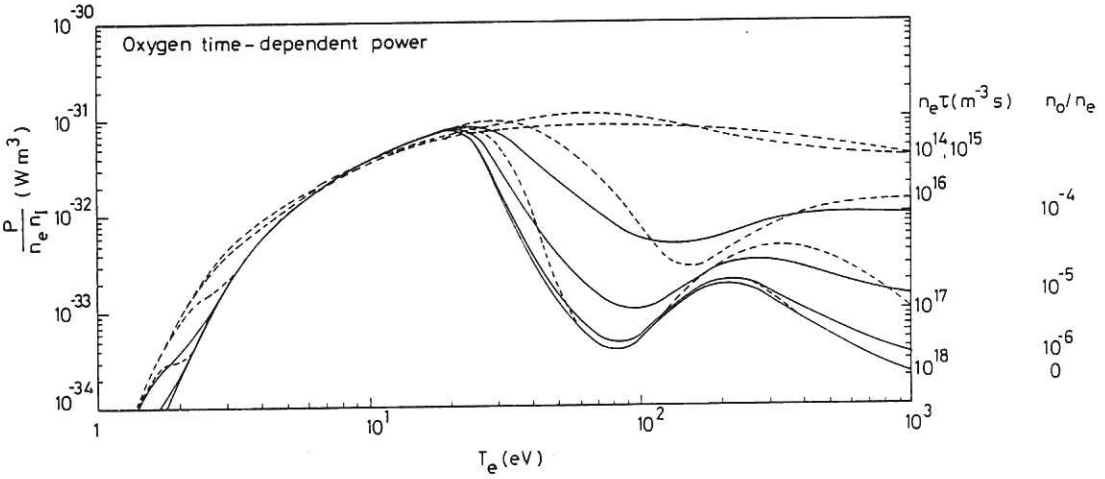

Fig.4(d) The oxygen radiation power functions, $P/(n_e n_I)$, at various values of $n_{e\tau}$(----) and the equilibrium functions with neutral hydrogen present (——).

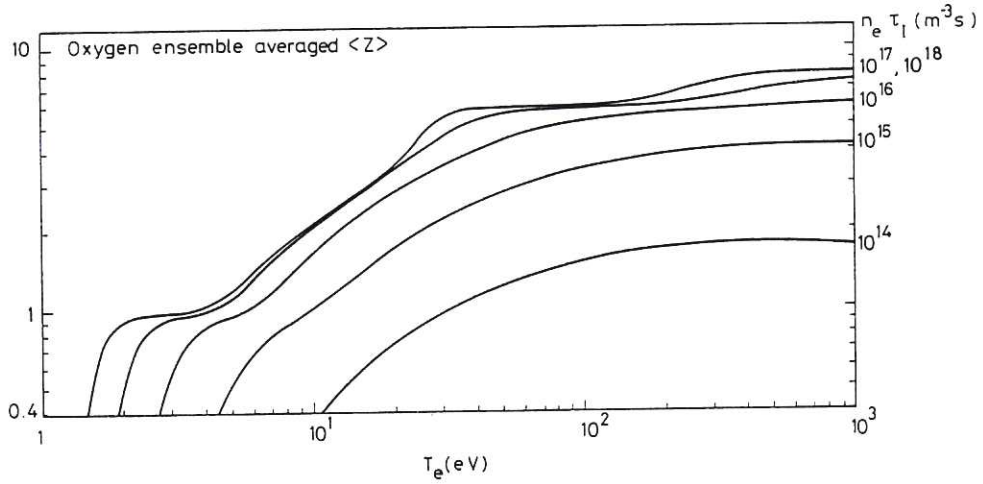

Fig.4(e) The oxygen time or ensemble averaged ionic charge, $<Z>$, for various values of τ_I (the impurity ion confinement time, or time in plasma).

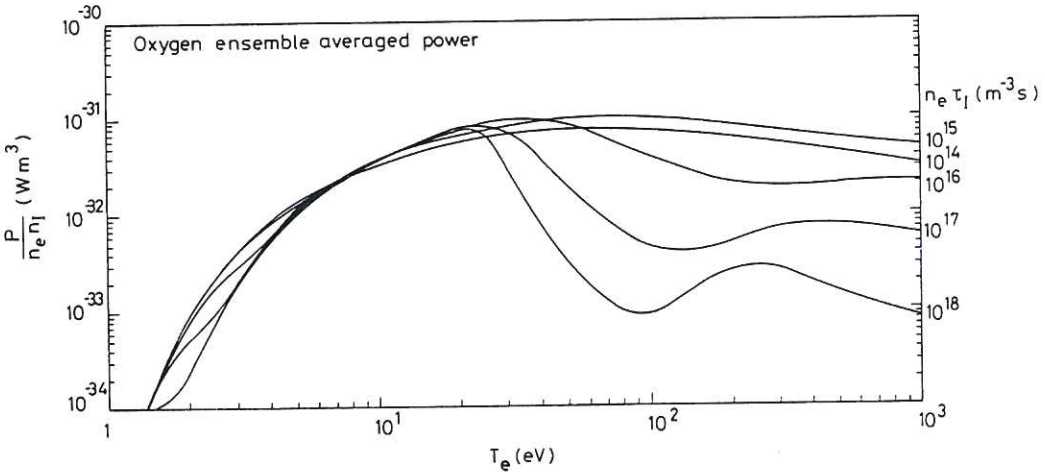

Fig.4(f) The oxygen time or ensemble averaged radiation power functions $P/(n_e n_I)$, for various values of τ_I (the impurity ion confinement time, or time in plasma).

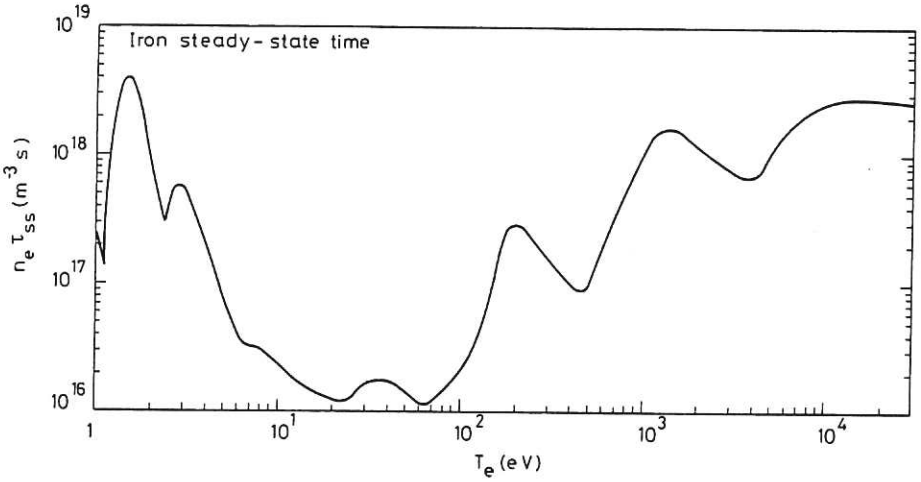

Fig.5(a) The $n_e\tau$ values for iron to reach a steady-state.

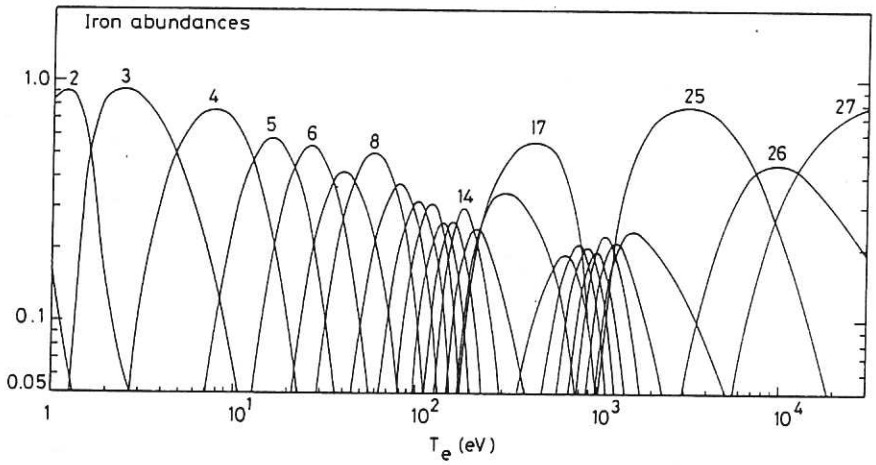

Fig 5(b) The iron equilibrium ionisation state distribution.

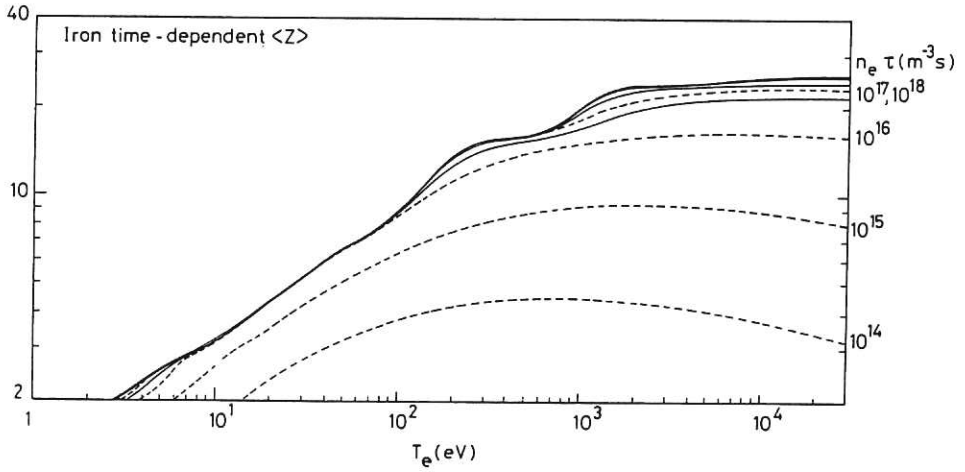

Fig.5(c) The iron mean ionic charge, <Z>, at various values of $n_e\tau$(----) and the equilibrium values with neutral hydrogen present (——).

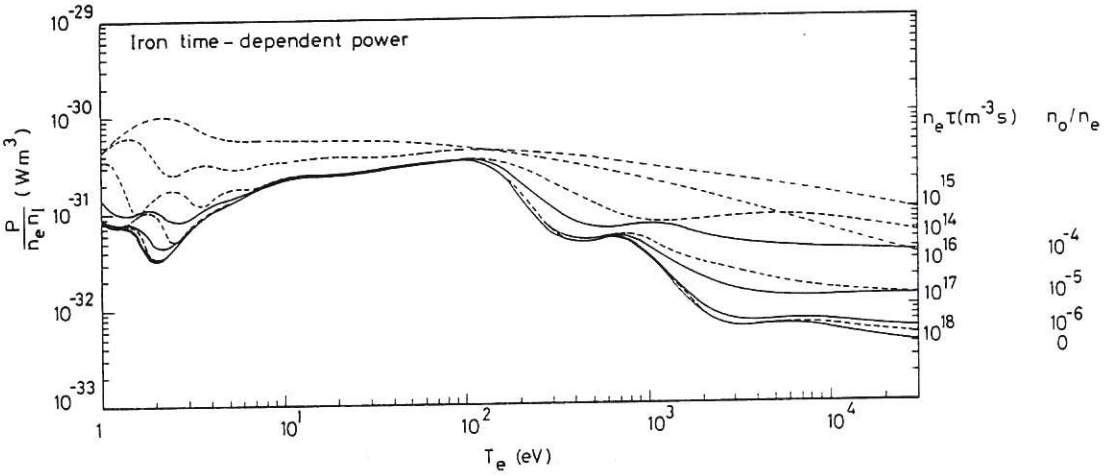

Fig.5(d) The iron radiation power functions, $P/(n_e n_I)$, at various values of $n_e\tau$(----) and the equilibrium functions with neutral hydrogen present (——).

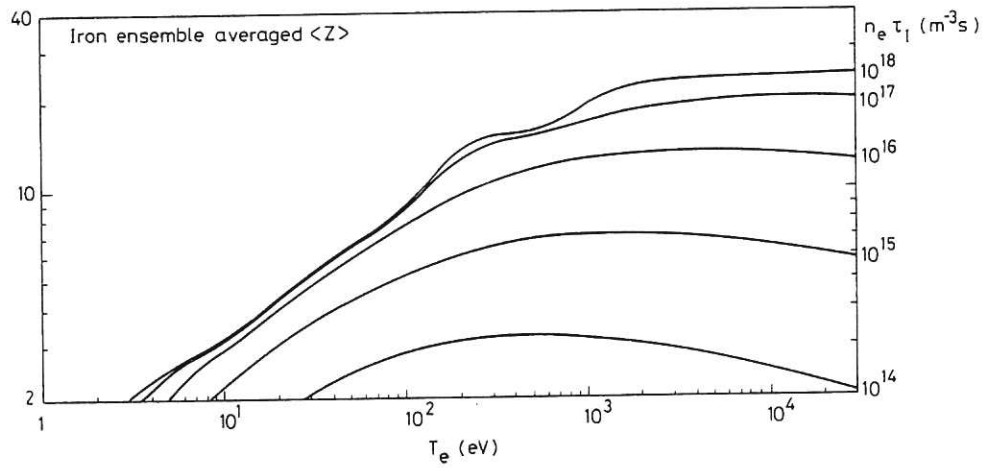

Fig.5(e) The iron time or ensemble averaged ionic charge, $<Z>$, for various values of τ_I (the impurity ion confinement time, or time in plasma).

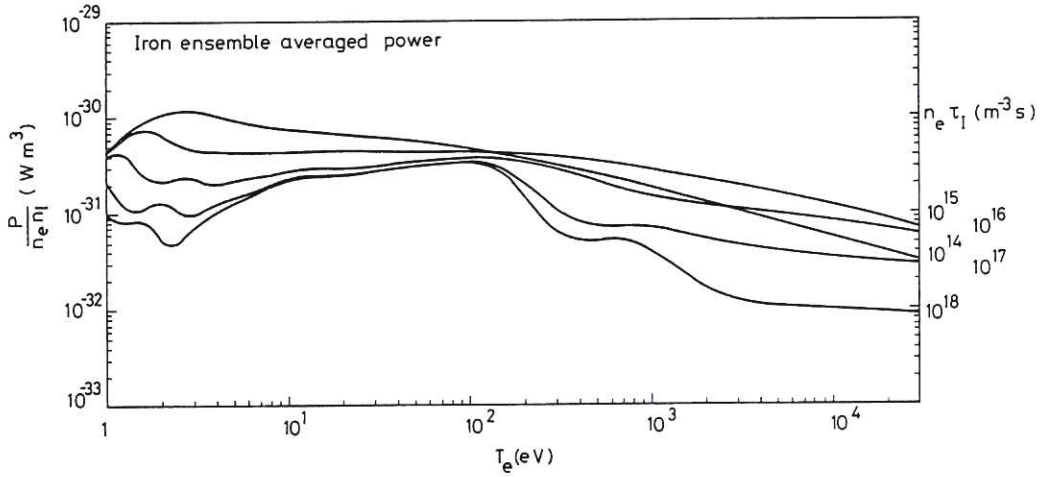

Fig.5(f) The iron time or ensemble averaged radiation power functions, $P/(n_e n_I)$, for various values of τ_I (the impurity ion confinement time, or time in plasma).

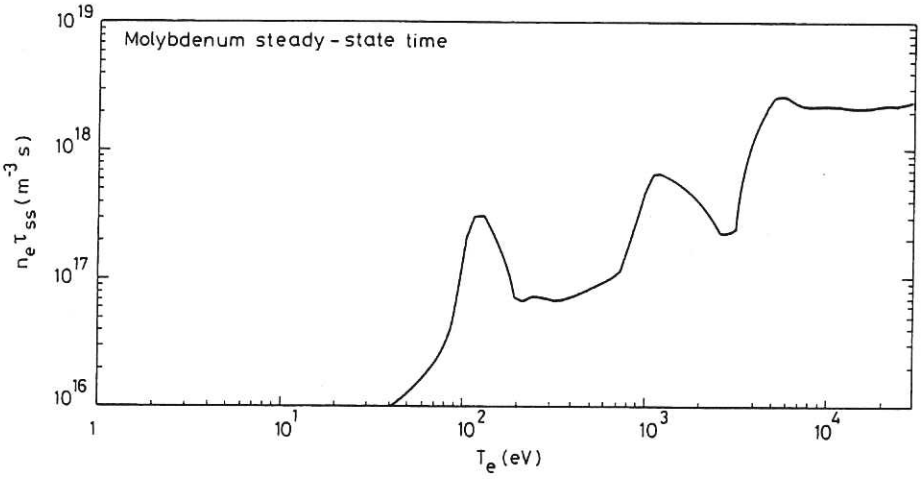

Fig.6(a) The $n_e\tau$ values for molybdenum to reach a steady-state.

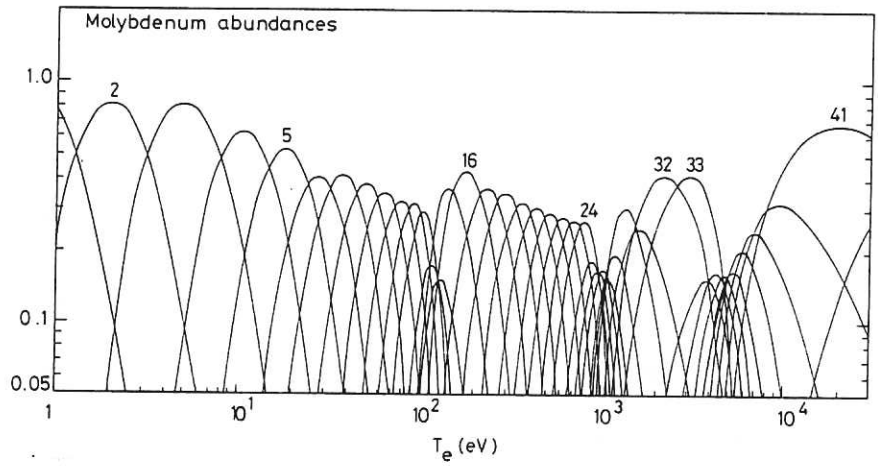

Fig.6(b) The molybdenum equilibrium ionisation state distribution.

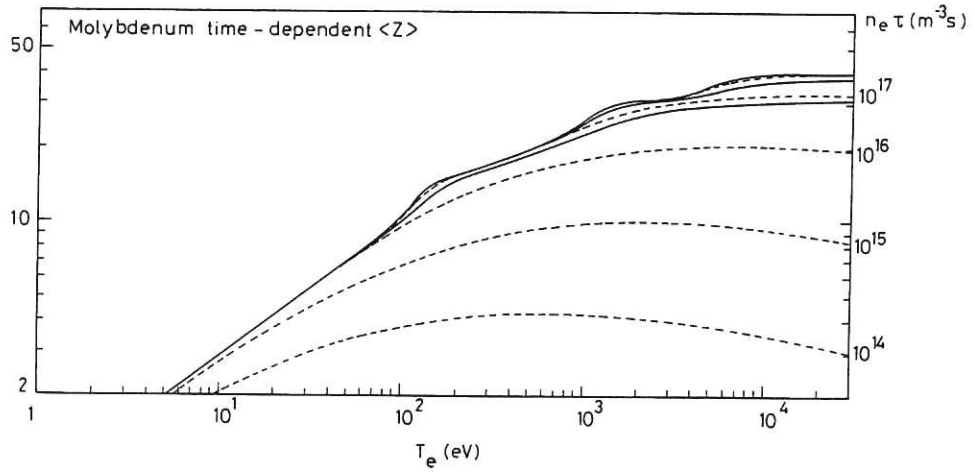

Fig.6(c) The molybdenum mean ionic charge, <Z>, at various values of $n_e\tau$(----) and the equilibrium values with neutral hydrogen present (——).

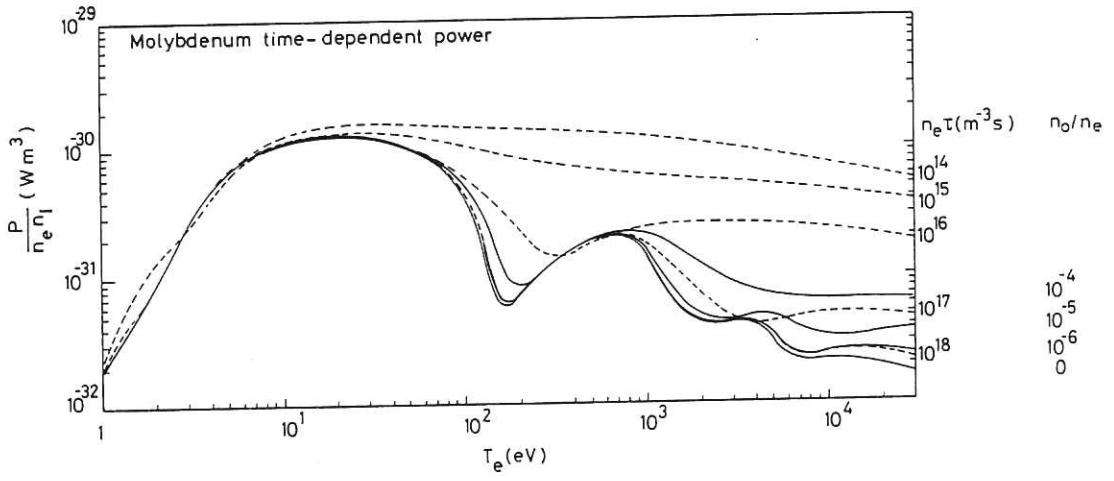

Fig.6(d) The molybdenum radiation power functions, $P/(n_e n_I)$, at various values of $n_e\tau$(----) and the equilibrium functions with neutral hydrogen present (——).

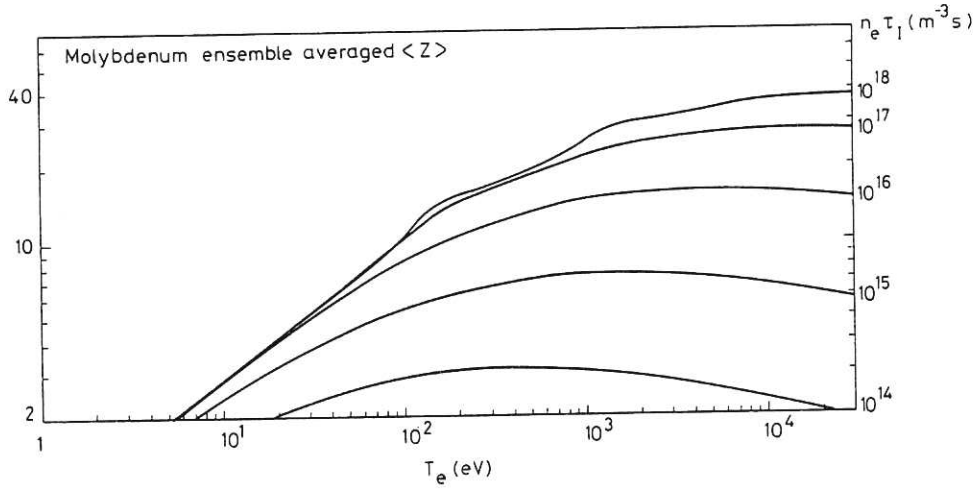

Fig.6(e) The molybdenum time or ensemble averaged ionic charge, <Z>, for various values of τ_I (the impurity ion confinement time, or time in plasma).

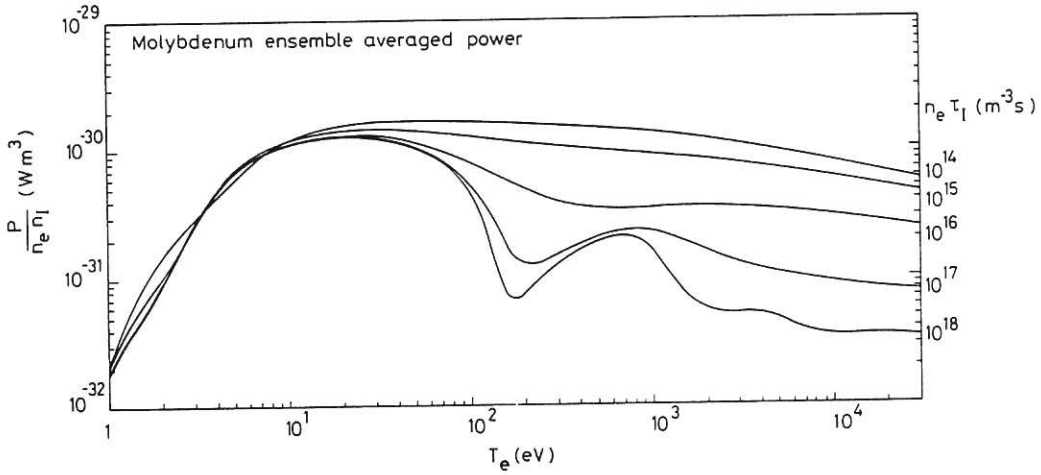

Fig.6(f) The molybdenum time or ensemble averaged radiation power functions, $P/(n_e n_I)$, for various values of τ_I (the impurity ion confinement time, or time in plasma).